Chapter 1

Introduction

In this introductory section, we explore the concept of phase separation in soft matter physical systems, coarse-graining methods, and the kinetics associated with these processes.

1.1 What is phase-separation?

Phase separation is a physical phenomenon in which a multicomponent system in a homogeneous mixed state separates into its distinct constituent phases [6–8]. These phenomena can occur in various systems, including metals, semiconductors, simple liquids, soft materials such as polymers, surfactants, colloids, biological materials, and food materials [9]. They play crucial roles in the domain evolution of immiscible multicomponent mixtures of any materials. These patterns are connected to the optical, electrical, and mechanical properties of the materials [10,11]. Based on the concept of dynamic universality in critical phenomena, phase separation in various condensed matter systems can be classified into two groups. Each group is characterized by a distinct set of fundamental equations that describe its dynamic process in phase-field models [12]. Phase separation in solids is referred to as the *model B* [10,12], while in fluids, it is known

as the *model H* [10,12] which described by the equations of linearized hydrodynamics [13]. However, the physical process for model H can lie under the different conditions such as variation in composition, tepmerature and pressure. Although phase separation is a process, it remains confined to laboratory-scale applications and is limited to several polymers [14].

This thesis mainly focuses on phase-separation in soft materials, e.g., polymeric melt, polymeric blend, and solutions of simple and polymeric fluid systems [7]. Soft materials frequently show a diverse and complex morphology having features from micro- to macroscopic length scales. Phase separation typically involves shifting from a less ordered to a more ordered state. The ordered state is quantified by the degree of randomness. This degree of randomness is measured using the thermodynamic parameter called entropy. A homogeneous mixed single state has a higher value of entropy compared to the ordered state has a smaller value of the entropy. The methodology of thr ordered parameter calculation is described in Sec. 1.3. Phase separation has significant applications in various fields, such as materials engineering for designing new materials, biotechnology for drug delivery and tissue engineering [15,16], and food technology for creating stable food emulsions [17]. There are various processes to achieve phase patterning of soft materials. However, self-assembly is a robust and fascinating treatment, which will be explored in the next section.

1.1.1 Self-assembly

When phase separation occurs due to local interactions among the components without any external assistance, it is referred to as self-assembly [6,18,19]. During this self-assembly process, the system's free energy is minimized [6]. The minimization of free energy can be categorized in two distinct ways. The first is static self-assembly, where the ordered state emerges as the system approaches equilibrium, thereby reducing its free

energy. The second involves dynamic self-assembly, where the ordered state forms under non-equilibrium conditions, such as forming non-equilibrium self-assembled structures, which often arise from phase transitions induced by alterations in temperature or pressure. Therefore, the formation of particular structures relies on the presence of a controlling parameter.

Thermodynamic perspective of self-assembly. In the realm of self-assembly, a delicate balance between entropy and enthalpy governs the segregation process. The appropriate free energy under constant temperature (T) and volume (V) is the Helmholtz free energy (F), defined as $F = U - TS$, where U signifies the internal energy of the system. The internal energy and the enthalpy (H) are related as: $H = U + PV$. At constant V, the change in enthalpy is equal to the change in internal energy, i.e., $\Delta H = \Delta U$. Given that F is a state parameter, transitioning from one state to another entails the change in F as $\Delta F = \Delta H - T\Delta S$. At a high temperature, entropy dominates over internal energy, making free energy minimum ($\Delta F < 0$). This leads to the homogeneously mixed state as the preferred equilibrium state. At a temperature below the critical temperature, entropy reduces due to lowered thermal fluctuation. As a result, the enthalpic contribution dominates over the entropic term. Therefore, minimizing free energy implies reducing enthalpy, which leads to ordering in various phases. Thus the enthalpy acts as a driving force, promoting phase separation and ordering subsequent phases, ultimately minimizing the Helmholtz free energy of the system [20].

1.2 Kinetics of phase-separation

To characterize the distinct phases and its behavior in self-assembly, we must induce significant changes in thermodynamic parameters, such as temperature or pressure, through processes like quenching [11,21–24]. A rapid change in temperature or pressure creates a fluctuation in the density of the system [25]. Nonequilibrium systems can be

categorized into two main classes: (1) driven systems that reach a steady state but never attain equilibrium, and (2) systems that relax towards an new equilibrium state [24,26]. Our focus is on the latter category—systems moving towards equilibrium. Before we continue, it is essential to define nonequilibrium or far-from-equilibrium systems. A system is considered far from equilibrium if its macroscopic variables (such as pressure and temperature) change over time or if there are macroscopic heat, mass, or charge currents [3]. This shifts the system away from its equilibrium state, leading to dynamic changes in morphology evolution. Exploring this class of problems involves understanding the *kinetics of phase-separation*, which can be quite fascinating [3,25,27]. The dynamics is interpreted through nonlinear evolution equations. Often, obtaining exact solutions for these time-dependent nonlinear evolutions is quite challenging. However, one effective analytical approach to understanding the resulting pattern dynamics is introducing domain boundaries or defects into the systems [3].

Phase separation can occur in systems within metastable and unstable regions, depending on the composition of the constituents. In the phase diagram, the boundary line separating the unstable region from the metastable region is known as the spinodal curve, while the boundary separating the metastable region from the stable region is known as the binodal curve [25].

Consider the phase diagram demonstrated in Fig. 1.2 for the binary simple mixture. The critical point is the location where the spinodal and binodal lines meet. The metastable region lies in between the binodal and spinodal lines. A large amplitude of fluctuations in free energy initiates phase separation in the metastable state. These fluctuations lead to the formation of tiny structures with a lower concentration than the initial mixture. These small structures are called nuclei, and their formation process is called *nucleation and growth* [25]. On the contrary, in an unstable state, any fluctuation, regardless of its amplitude, lowers free energy, thereby triggering phase separation. Since

small-amplitude density fluctuations are consistently present throughout the system, phase separation in the unstable state happens instantly; this segregation process is known as *spinodal decomposition* [25]. Systems with critical or near-critical compositions can undergo phase segregation through spinodal decomposition. For a general overview, refer to the references [3,11,21,24,28].

Since the early 1960s, phase ordering kinetics has been the subject of extensive research. It has a long-standing history that began with the work of Cahn and Hilliard [29]. Some crucial studies on the kinetics of phase separation during the initial stages include the pioneering work by Lifshitz and Slyozov [30], Wagner [31], and Lifshitz [32]. However, observing the scaling law using Monte Carlo simulations has intensified the focus of the study [33–38]. Afterwards, in the 1990s, significant advancements were made through the contributions of Furukawa [39], and Binder [40], Lager [41]. The phase segregation dynamics occur in diverse contexts, ranging from the clustering dynamics of the early universe to the formation of tiny structures (e.g., nanostructures). Moreover, phase ordering in systems including liquid helium, ferromagnets, antiferromagnets, and liquid crystals has been researched and explored theoretically and experimentally [42–44].

1.2.1 Phase diagram

The domain growth is explored with a typical example of the simple binary fluids, which consist of two incompatible fluid particles/molecules. To show the domain growth, rapidly change the thermodynamic parameters like temperature or pressure from a high value to below the critical value of the system. This abrupt change in temperature or pressure is referred to as quenching in the system. In temperature quenching, we consider the desired temperature T below the critical temperature T_c. However, T can be considered below or above T_c for the quench depending on the phase separating system. The phase segregation of polymer solutions, determined by two quenching criteria, is crucial in

the research, development, and design of various polymer-based soft materials [1–3,45]. These solubility limits are known as the lower critical solution temperature (LCST) and upper critical solution temperature (UCST), as will be described in the following sections.

1.2.2 Lower critical solution temperature (LCST)

A homogeneous mixed state exists at some lower temperature compared to the critical temperature of the system, and elevation of the system's temperature leads to the formation of two immiscible phases. This phase separation lies under a *lower critical solution temperature* (LCST) limit. The phase diagram for this LCST limit is shown in Fig. 1.1. The binodal line separates the homogeneous mixed phase from the metastable state, while the spinodal line separates the miscibility gap from the metastable state. A system with critical composition (equal proportion of constituents) is decomposed via the spinodal line, whereas phase segregation of off-critical composition (unequal proportion of constituents) is provided via nucleation and growth.

Certain polymers in water solvent undergo phase separation as the temperature rises. The polymer is dissolved in water at lower temperatures and remains hydrated because of hydrogen bond formation. As the temperature increases, the polymer loses its hydration due to breaking the weaker hydrogen bonds, causing the polymer to aggregate. The abrupt shift from hydrophilic (water loving) to hydrophobic behavior is caused by the presence of hydrogen bonds [45]. Thermoresponsive polymer solutions, such as poly(methoxydiethylene glycol methacrylate) (PmDEGMA) and poly(methoxytriethylene glycol methacrylate) (PmTEGMA) [1], undergo phase segregation when the temperature increases.

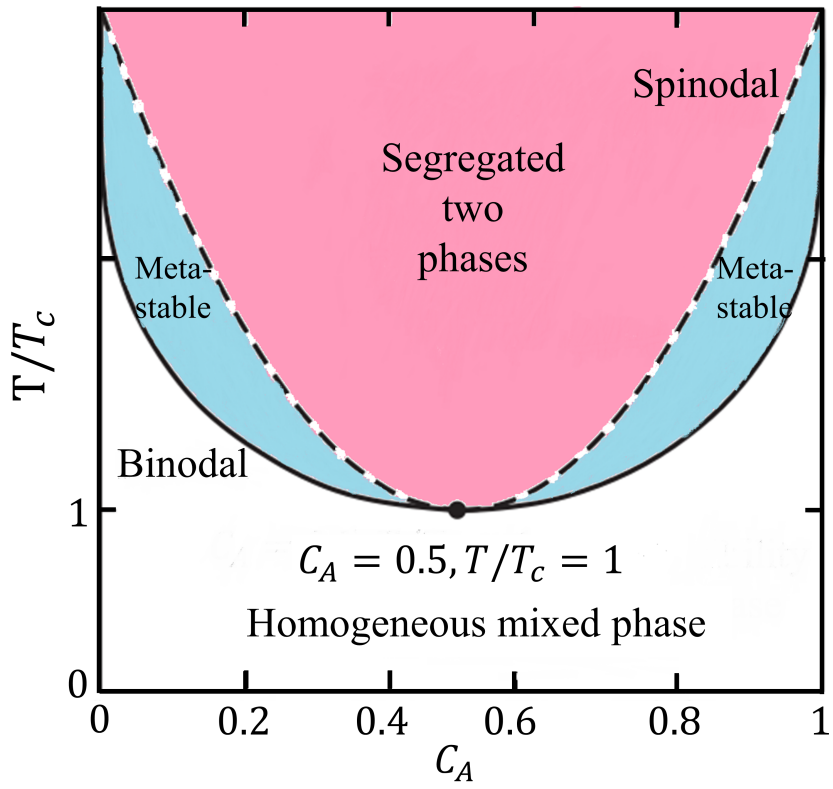

Fig. 1.1: A schematic depicting the phase diagram of a simple binary (AB) mixture with a lower critical solution temperature (LCST) limit. The system parameters are defined in terms of the concentration of entity A ($C_A = 1 - C_B$) and the temperature (T). It illustrates two equilibrium phases: a homogeneous phase and segregated phases, separated by two curves: the binodal (solid line) and the spinodal (dashed line). The system is segregated and characterized by regions enriched in A and B phases [1,2].

1.2.3 Upper critical solution temperature (UCST)

When a polymeric system is heated beyond its transition (or critical) temperature, the components of the mixture become uniformly miscible, forming a homogeneous mixed single state. Entropy is the driving factor in regulating the phase equilibrium state. However, upon rapidly decrease to temperatures below the transition temperature, the constituent phases undergo segregation. This phase segregation lies under the *upper critical solution temperature* (UCST) limits. Fig. 1.2 depicts the phase diagram indicating the segregation limit associated with the UCST in simple binary fluids.

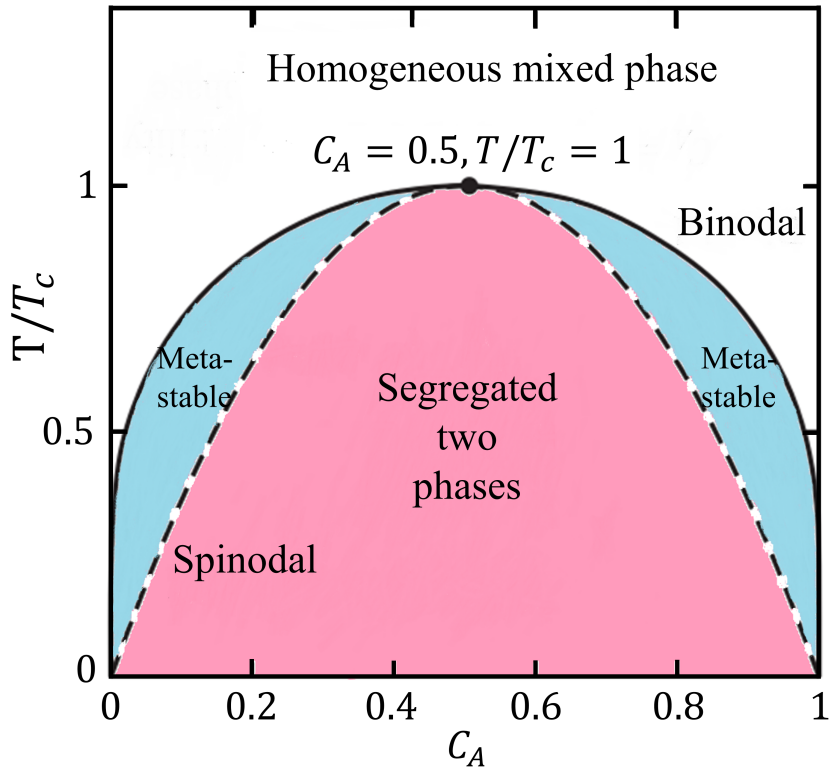

Fig. 1.2: A schematic depicting the phase diagram of a simple binary (AB) mixture with a upper critical solution temperature (UCST) limit. The system parameters are defined in terms of the concentration of entity A ($C_A = 1 - C_B$) and the temperature (T). It illustrates two equilibrium phases: a homogeneous phase and segregated phases, separated by two curves: the binodal (solid line) and the spinodal (dashed line). The system is segregated and characterized by regions enriched in A and B phases [3].

Simple binary (AB) fluids mixture provides frameworks for understanding the dynamics of phase ordering below the trasnition temperature. To achieve phase segregation, minimize the Helmholtz free energy $F(T, \psi)$, where ψ represents the difference in number concentration between the two fluids. Attractive interactions occur between particles of the same type AA or BB, while dissimilar (A-B) type particles exhibit repulsive interaction. The system kinetically separates into regions enriched with A and B phases. At $t = 0$ ($T > T_c$), the system is in a mixed single state and is rapidly quenched below the coexistence curves. This sudden change renders the system thermodynamically unstable, prompting local rearrangements to relax within this transient regime. An inhomogeneous

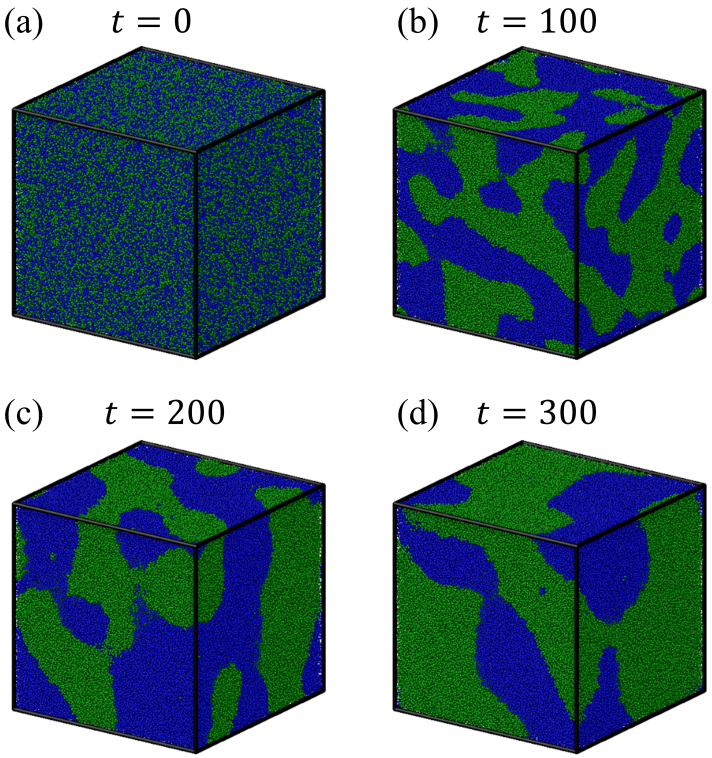

Fig. 1.3: The phase ordering and temporal evolution snapshots depict a simple binary (AB) mixture. Snapshot (a) at $t = 0$ shows a uniformly mixed state, while, snapshots (b), (c), and (d) represent time evolution at three distinct times. The quenched temperature is set at $T = 1$ (in a reduced DPD unit). These evolution snapshots are derived from DPD simulations in $d = 3$. The blue and green regions signify A- and B-rich phases, respectively.

state of macroscopic density progresses into two separate phases. Afterward, the system undergoes phase segregation enrichment of phases A (blue region) and B (green region) via minimizing in Helmholtz free energy. The domain coarsening is depicted in Fig. 1.3, in which evolution snapshots show three different times. The time-dependent evolution of this macroscopic density is the quantity of interest and the number of A and B molecules would remain conserved separately.

1.3 Landau theory

In domain coarsening, an entity that characterizes the ordering of phases, is referred as the order parameter of the system. Concerning the UCST limit, an order parameter is non-zero below the transition temperature T and becomes zero above it. For example, ferromagnetic materials have an ordering of magnetization density (magnetic moments per unit valome), and polymeric fluids have an ordering of density (number of particles per unit volume). Gorsky-Bragg-Williams [46] initially proposed to explain order-disorder transitions in alloys. Further, Landau subsequently formulated a phenomenological approach utilizing free energy to describe phase transitions [47,48]. It represents an intensive thermodynamic variable. The spatial extent of this ordering is quantified by a parameter referred to as the correlation length.

It presents a generic phenomenological theory of a second-order continuous phase transitions. The essential point in framing Landau's theory is to describe the Gibbs free energy $G(\psi(\vec{r}), T)$ of a system in the vicinity of its phase transition, where $\psi(\vec{r})$ is the local order parameter at temperature T [43]. This theory focuses on macroscopic behavior associated with order parameters, $\psi(\vec{r}, t)$, at position $\vec{r}$ and time t. The free energy of the system is expanded in powers of the order parameter, typically up to fourth order, with coefficients that depend on temperature and other relevant variables. The Gibbs free energy must remain unchanged when subjected to all Hamiltonian symmetry operations and associated with all combinations of $\psi(\vec{r})$.

A typical form of $G(\psi(\vec{r}), T)$ is:

$$G(\psi(\vec{r}), T) = \frac{A}{2}\psi^2 + \frac{B}{4}\psi^4 + O(\psi^6), \tag{1.1}$$

where coefficients A and B are the temperature-dependent phenomenological parameters, $O(\psi^6)$ is the higher order terms. For thermodynamic stability of the system, the coefficient

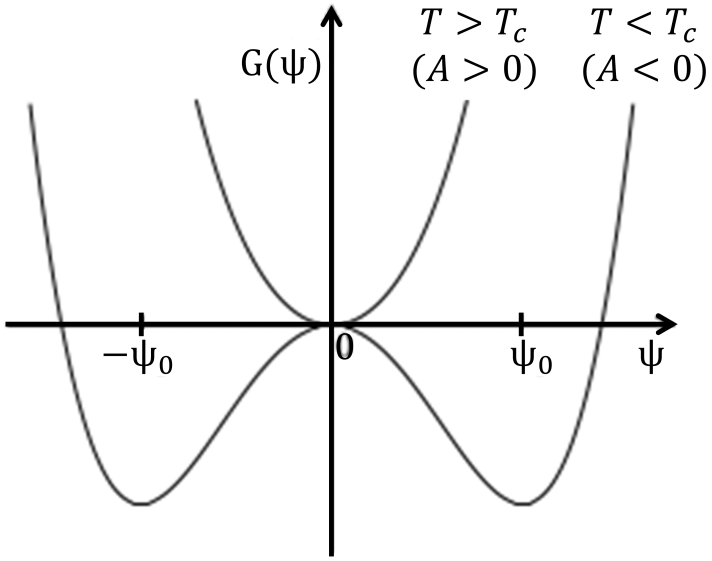

Fig. 1.4: The Landau free-energy density $G(\psi)$, expressed as a function of ψ, exhibits distinct behaviors based on the sign of A. When $A > 0$, the global minimum is located at $\psi = 0$, representing a homogeneous single phase. Conversely, when $A < 0$, degenerate global minima occur at $\psi_0 = \pm\sqrt{-A/B}$, illustrating the equilibrium state where two phases coexist [4,5].

of the highest even power of the order parameter should be positive, $B > 0$. A crucial aspect of this free energy density depends on the sign of $A \simeq A_0(T - T_c)$, where A_0 is positive. In Fig. 1.4, the free energy density above the transition temperature (where $A > 0$) is positive, indicating a uniform mixed phase, while it becomes negative ($A < 0$) at lower temperatures ($T < T_c$) exhibiting two equilibrium phases [4,5].

1.4 The dynamical scaling hypothesis

When a disordered state is quenched below the transition temperature, the system undergoes thermodynamic instability. Constituents begin to order and grow richer over time. The phase-segregation takes place as a result of minimizing the free energy and decreasing the interfacial energy. The domains coarsening possess a characteristic length scale $L(t)$, which increases as time progresses. The dynamical scaling hypothesis suggests

that this typical characteristics length scale, $L(t)$, characterizes all dynamical aspects of the structure. The system becomes statistically independent over time by scaling the domain size by corresponding $L(t)$. The law governing the subsequent growth is comprehensively understood only in the asymptotic limit of the phase ordering process.

Regarding morphology characterization, two commonly utilized physical observables that describe statistical variables of experimental relevance are the two-point equal-time pair correlation function [3,11,21,24] defined as:

$$C(\vec{r},t) = \left\langle \psi\left(\vec{R}+\vec{r},t\right)\ \psi\left(\vec{R},t\right)\right\rangle, \tag{1.2}$$

and its Fourier transform, known as the structure factor [3,11,21,24]:

$$S(\vec{k},t) = \left\langle \psi\left(\vec{k},t\right)\ \psi^{\star}\left(\vec{k},t\right)\right\rangle. \tag{1.3}$$

Here $\langle\cdots\rangle$ indicates averaging over initial conditions and thermal fluctuations, $\vec{k}$ is the wave-vector in Fourier space. A single characteristic length scale, L, indicates that the correlation function and the structural factor follow scaling forms, according to the scaling hypothesis [3,21] :

$$C(\vec{r},t) = g\left(\frac{r}{L}\right), \tag{1.4}$$

$$S(\vec{k},t) = L^{d} f\left(kL\right), \tag{1.5}$$

where d is the spatial dimentionality, $g(x)$ and $f(p)$ are scaling functions. The eq. 1.5 are well followed by the experimental as well as simultaion data.

In Fig. 1.5, we show the unscaled and scaled correlation and structure factor data plots for the simple binary fluids at three different times by utilizing the DPD simulation technique (see Sec. 2.1). Fig. 1.5(a) shows the correlation function shifts towards a higher value of the r. We scaled the $C(r,t)$ datasheets with the characteristics length

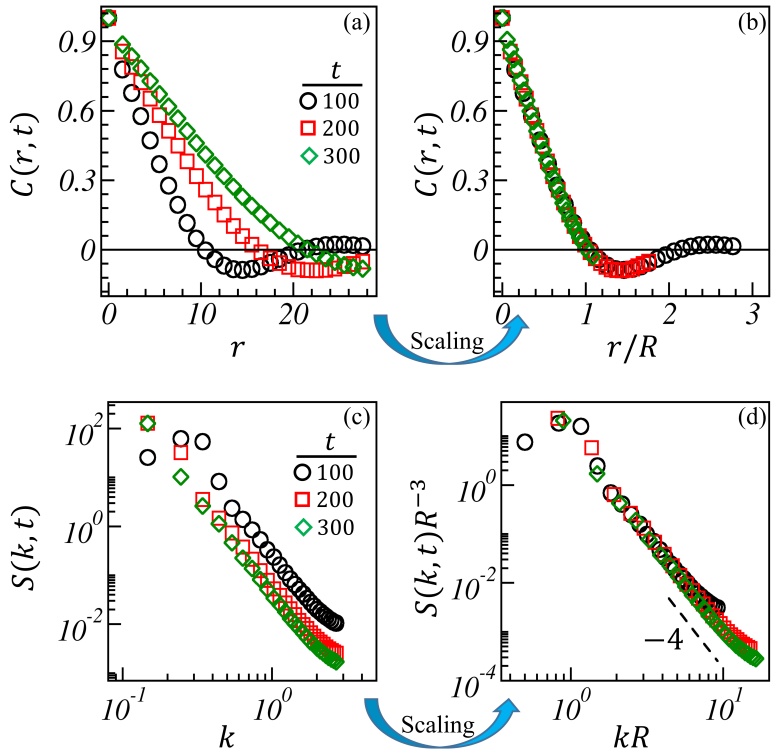

Fig. 1.5: Plot (a) shows the unscaled correlation function, while its scaled form is shown in (b). Plot (c) displays the unscaled structure factor, with its scaled form depicted in (d) at three different times $t = 100,\ 200$, and 300, corresponding to the evolution snapshots of Fig. 1.3.

R and observed that all curves overlapped onto each other as shown in Fig. 1.5(b). The overlapping of all curves shows that they belong to the same universality class. In Fig. 1.5(c), we plot the corresponding unscaled structure factor, $S(k,t)$ vs. k, on a log-log scale for three different times and the scaled structure factor plot as shown in Fig. 1.5(d).

Characteristic length scale. We can estimate the characteristic length scale using (1) from the correlation function and (2) from the structure factor. Firstly, the characteristic length scale (L) can be defined as the distance over which the correlation function $C(r,t)$ decays to 0.2 from its maximum value [3]. Secondly, from the structure factor function, Binder, Stauffer, and Furukawa [49–51] propose an expression for $S(\vec{k},t)$ in terms of the wave vector when the interface thickness is much smaller than the pattern

size.

$$S(\vec{k},t) = [\langle k\rangle\,(t)]^{-d} f\left(\vec{k}/\langle k\rangle L\right), \tag{1.6}$$

where $\langle k\rangle\,(t)$ represents the first moment of the scaled structure factor. The inverse of the first moment signifies the pattern size, denoted as $\langle k\rangle\,(t)^{-1} = L(t)$, and it asymptotically follows a power law: $\langle k\rangle\,(t)^{-1} \sim t^{\phi}$, where ϕ is the growth exponent (see Sec. 1.5 for more details).

1.4.1 Porod's law

This law describes the singular behavior of the correlation function in the limit of $r \to 0$ and the corresponding tail behavior of the structure factor in Fourier space. In this regards, as $r \to 0$, the correlation function decays linearly as

$$C(r,t) = 1 - ar^{\eta}\cdots, \tag{1.7}$$

where a is a constant factor and η is an exponent. For a pure phase separating system, $\eta = 1$ is obtained from the scattering off sharp interfaces [3,21,52,53]. The sharp interfaces or defects correspond to the correlation function's short-distance singularity, as Eq. 1.7 describes. This short-distance singularity plays a crucial role in determining the behavior of the structure factor at a large wave vector, k. The Fourier transform of Eq. 1.7 in d-dimensional space results in a power-law decay, defined as

$$S(k,t) \sim L^{d}\frac{A_d}{(k)^{(d+1)}},\ k \to \infty. \tag{1.8}$$

This significant result, the Porod law, was first established for scattering in two-phase systems [53]. Here, A_d represents the amplitude of the Porod tail [3]. Equations 1.7 and 1.8 are used to estimate the interface properties of domains in phase-separating systems.

In Fig. 1.5(d), we plot the scaled structure factor, $S(k,t)R^{-3}$, as a function of kR for binary simple fluids. The slope of -4 at large values of k (i.e., $k \to \infty$) indicates that the domain interfaces are smooth and conform to the Porod law.

1.5 Domain growth law

The scaling hypothesis proposes a perceptive method to derive the growth laws for $L(t)$. Consider a single characteristic length L, utilize the Allen-Cahn equation [29], and define the domain wall velocity (in the direction of increasing order parameter ϕ) of a nonconserved fields system (Model A). The interfacial velocity v is defined as follows

$$t \sim \frac{L(t)}{v}. \tag{1.9}$$

The domain wall velocity is computed using the $v \sim dL/dt$ equation. The curve surface is near the domain wall, defined as mean curvature, K. For a spherical domain, the curvature is defined as $K \sim \frac{d-1}{L(t)}$, where d is the dimensionality. This can be simplified to $K \sim \frac{1}{L(t)}$. Further evaluation of the characteristics length, we get

$$L(t) \sim t^{1/2}. \tag{1.10}$$

This relation satisfies for the nonconserved scaler order parameter fields and is referred to as the Allen-Cahn growth law.

Now considering the conserved fields (Model B), and following the approach of Huse, the chemical potential has a typical form $\mu \sim \sigma/L$, here σ is the surface tension and varies over a length scale of order L. This leads to a concentration gradient $|\nabla\mu| \sim \sigma/L^2$. We can estimate the resulting diffusion current as $dL(t)/dt$, which leads to the growth of

the domains. Thus, we obtain

$$\frac{dL(t)}{dt} \sim \frac{\sigma}{L(t)^2}, \tag{1.11}$$

integrating this gives us the growth law

$$L(t) \sim (\sigma t)^{1/3}. \tag{1.12}$$

This growth law is referred in the literature as the Lifshitz-Slyozov growth law [30]. This physical mechanism includes vaporizing material from smaller droplets followed by condensation onto larger droplets.

The segregation dynamics in binary simple liquids is a patterning phenomenon of significant experimental interest. Model B (conserved order parameter) is unsuitable for this system because it needs to consider the transport of the order parameter by hydrodynamic flow. For appropriate modification with included the local fluid velocity, $\vec{v}$ term in the continuity equation

$$\frac{\delta\phi}{\delta t} + \vec{v}.\vec{\nabla}\psi = \lambda\nabla^2\mu. \tag{1.13}$$

Here λ is the transport coefficient and ψ is the order parameter. This velocity field obeys the Navier-stokes equation, and fluid behaves as an incompressible and follows the appropriate equation

$$\rho\left(\frac{\delta\vec{v}}{\delta t} + (\vec{v}\cdot\vec{\nabla})\vec{v}\right) = \eta\nabla^2\vec{v} - \vec{\nabla}p - \psi\vec{\nabla}\mu. \tag{1.14}$$

where ρ is the density of incompressible fluid, p and η represent pressure and the fluid viscosity. The last term in Eq. 1.14 results from the free-energy change of approximately $\psi\delta\mu$ per unit volume, which occurs when a fluid region with an order parameter ψ is transported over a distance where the chemical potential changes by $\delta\mu$. This implies

that gradients in the chemical potential provide a driving force on the fluid. The incompressibility condition imposes a constraint on the velocity field, requiring that $\vec{\nabla} \cdot \vec{v} = 0$. Relevant to the most experimental systems, the dynamics of the velocity field are much faster than those of the order-parameter field, thus left hand side of Eq. 1.14 can be set to zero, i.e. $\delta\vec{v}/dt = 0$. Moreover, the solution of the velocity in Fourier space

$$v_\alpha(k) = T_{\alpha\beta}(k) F_\beta(k). \tag{1.15}$$

$$T_{\alpha\beta}(k) = \frac{1}{\eta k^2}\left(\delta_{\alpha\beta} - \frac{k_\alpha k_\beta}{k^2}\right). \tag{1.16}$$

where $F = -\psi\nabla\mu$. The α, and β are indices. The parameter $T_{\alpha\beta}(k)$ is the Oseen tensor in Fourier space. In $d = 3$, Oseen tensor express in real space as

$$T_{\alpha\beta}(r) = \frac{1}{8\pi\eta r}\left(\delta_{\alpha\beta} + \frac{r_\alpha r_\beta}{r^2}\right). \tag{1.17}$$

substituting the expression for the velocity from Eq. 1.15 in real space with the order parameter,

$$\frac{\delta\psi}{\delta t} = \lambda\nabla^2\mu - \int d\vec{r'}\left[\nabla\psi(r)\cdot T(\vec{r}-\vec{r'})\cdot\nabla'\psi(\vec{r'})\right]\mu(\vec{r'}). \tag{1.18}$$

It is crucial to emphasize that Eq. 1.18 neglects thermal fluctuations. Asymptotic scaling is governed by strong-coupling.

Using dimensional arguments to estimate the domain coarseing asymptotic limit. The Eq. 1.18 can be utilized to comprehend the domain growth laws for coarsening in binary fluids. In the initial stages, growth is driven by diffusion, similar to the behavior observed in binary alloys. However, as the regime shifts to hydrodynamic growth, advection quickly transports the material along domain boundaries [27,30,39]. Its behavior is intended to approach specific characteristics asymptotically. Bray [21] provides a summary of growth

laws applicable to various regimes:

$$L(t) \simeq \begin{cases} (D\sigma t)^{1/3}, & L \ll (D\eta)^{1/2}, \text{(diffusive regime)} \\ \frac{\sigma t}{\eta}, & (D\eta)^{1/2} \ll L \ll \frac{\eta^2}{\rho\sigma}, \text{(viscous hydrodynamic regime)} \\ \left(\frac{\sigma t^2}{\rho}\right)^{1/3}, & \frac{\eta^2}{\rho\sigma} \ll L, \text{(inertial hydrodynamic regime)} \end{cases} \tag{1.19}$$

The physical origin of the linear growth observed in the viscous hydrodynamic regime has been investigated by Siggia [27]. He describes the fundamental mechanism as the movement of hydrodynamic fluids driven by surface tension along the interface.

1.6 Overview of the thesis

We provide an outline of the chapters in this thesis before summarizing this chapter. In *Chapter 2*, we present the simulation technique used in work described in the chapters 3, 4, 5 and 6. Among the various techniques available, we employ a mesoscopic method known as DPD. This method operates at a length scale that bridges the gap between atomistic and macroscopic scales.

In *Chapter 3*, we study the kinetics of phase separation in a binary simple fluid. We introduce an amphiphilic polymer as a solute at the boundaries of the simple fluid domains. We analyze the density profile and the radial distribution function of the simple fluids. Additionally, we discussed the two-point equal-time correlation function, and its Fourier transform is the structure factor to understand the effect of various amphiphilic polymer topologies, their flexibility and the size. Furthermore, we estimate how the domain growth scaling function emerges. We observe that the scaled length follows a crossover from a diffusion-dominated regime ($\phi = 1/3$) to a saturation regime ($\phi = 0$).

In *Chapter 4*, we extend our previous study on the segregation kinetics of BCP melt systems by tuning external stimuli, such as light. The light was applied in a sequence

of on-cycle and off-cycle. In this work we use a combination of equal and unequal time limits for the off-cycles while on-cycles was kept for the same period. We highlight the dynamic scaling functions and the formation of evolution morphology, which results in a bicontinuous frozen structure instead of the usual lamellar.

In *Chapter 5*, we investigate the influence of polymeric components at the domain interface of binary simple fluids. This work extends the study of Chapter 3, where we focused on amphiphilic polymers at the simple fluid interface. To comprehensively describe this study, we adjust the concentration of polymeric components, vary their affinities, stiffness and rigidity, and alter the polymer chain length. We characterize the evolving morphology using various physical observables, such as the radial distribution and dynamical scaling functions.

In *Chapter 6*, we consider three different block copolymer melt systems that vary in chain topology. We study how morphology changes by tuning the composition ratio of BCP components. To observe the spatial distribution of these emerging morphologies, we analyze the radial distribution function (RDF) and for the polymer size during the evolution process, we compute the radius of gyration. To characterize the morphologies, we use the dynamic scaling functions, the two-point equal-time correlation function, its momentum space counterpart, the structure factor, and the characteristic length scale.

1.7 Summary and conclusions

In this chapter, we present a broad discussion on the self-assembly mechanism and domain coarsening for two different types of phase diagram limits: (a) Lower critical solution temperature (LCST) and (b) Upper critical solution temperature (UCST). We also provide an overview of phase separation kinetics using the example of a simple binary fluid mixture under the UCST limit. The evolution of morphology is characterized by the emergence and growth of domains enriched in different components of the mixture.

We explore the growth laws that describe domain growth kinetics, where the average size of the clusters follows a power law dependence over time as $L(t) \sim t^{\phi}$, where ϕ is the growth exponent. Moreover, we discuss dynamic scaling functions such as the two-point equal-time correlation function and its momentum space transformation, the structure factor. This chapter provides a qualitative understanding of the theoretical tools used to characterize morphology, which will be applied in subsequent chapters.